

## Observation of an intermediate to H<sub>2</sub> binding in a metal–organic framework

Brandon R. Barnett<sup>1,2</sup>, Hayden A. Evans<sup>3</sup>, Gregory M. Su<sup>4</sup>, Henry Z. H. Jiang<sup>1,2</sup>, Romit Chakraborty<sup>1,2</sup>, Didier Banyeretse<sup>5</sup>, Tyler J. Hartman<sup>5</sup>, Madison B. Martinez<sup>6</sup>, Benjamin A. Trump<sup>3</sup>, Jacob D. Tarver<sup>3</sup>, Matthew N. Dods<sup>7</sup>, Walter S. Drisdell<sup>4</sup>, Katherine E. Hurst<sup>6</sup>, Thomas Gennett<sup>6,8</sup>, Stephen A. FitzGerald<sup>5</sup>, Craig M. Brown<sup>3,9</sup>, Martin Head-Gordon<sup>1,4</sup>, and Jeffrey R. Long<sup>1,2,7\*</sup>

<sup>1</sup>Department of Chemistry, University of California, Berkeley, Berkeley, California 94720, United States

<sup>2</sup>Materials Sciences Division, Lawrence Berkeley National Laboratory, Berkeley, California, 94720, United States

<sup>3</sup>Center for Neutron Research, National Institute of Standards and Technology, Gaithersburg, Maryland 20899, United States

<sup>4</sup>Chemical Sciences Division, Lawrence Berkeley National Laboratory, Berkeley, California 94720, United States

<sup>5</sup>Department of Physics, Oberlin College, Oberlin, Ohio 44074, United States

<sup>6</sup>Chemistry & Nanoscience Center, National Renewable Energy Laboratory, Golden, Colorado 80401, United States

<sup>7</sup>Department of Chemical and Biomolecular Engineering, University of California, Berkeley, Berkeley, California 94720, United States

<sup>8</sup>Department of Chemistry, Colorado School of Mines, Golden, Colorado 80401, United States

<sup>9</sup>Chemical and Biomolecular Engineering, University of Delaware, Newark, Delaware 19716, United States

\*Correspondence to: [jrlong@berkeley.edu](mailto:jrlong@berkeley.edu) (J. R. L.)

**Coordinatively-unsaturated metal sites within certain zeolites and metal–organic frameworks can strongly adsorb various molecules<sup>1-4</sup>. While many classical examples involve electron-poor metal cations that interact with adsorbates largely through electrostatic interactions, unsaturated electron-rich metal centers housed within porous frameworks can often chemisorb guests amenable to redox activity or covalent bond formation.<sup>5-9</sup> Despite the promise that materials bearing such sites hold in addressing myriad challenges in gas separations and storage<sup>10-12</sup>, very few studies have directly interrogated mechanisms of chemisorption at open metal sites within porous frameworks. Here, we show that H<sub>2</sub> chemisorption at the trigonal pyramidal Cu<sup>+</sup> sites in the metal–organic framework Cu<sup>I</sup>-MFU-4l<sup>13</sup> occurs via the intermediacy of a metastable physisorbed precursor species. *In situ* powder neutron diffraction experiments enable crystallographic characterization of this intermediate, the first time that this has been accomplished for any material. Support for a precursor intermediate is also afforded from temperature-programmed desorption and density functional theory calculations. The activation barrier separating the precursor species from the chemisorbed state is shown to correlate with a change in the Cu<sup>+</sup> coordination environment that enhances  $\pi$ -backbonding with H<sub>2</sub>. Ultimately, these findings demonstrate that adsorption at framework metal sites does not always follow a concerted pathway and underscore the importance of probing kinetics in the design of next-generation adsorbents.**

The chemisorption of small diatomic molecules such as H<sub>2</sub>, N<sub>2</sub>, O<sub>2</sub>, CO, and NO on metal surfaces has been thoroughly studied, owing its relevance to important catalytic cycles<sup>14-15</sup>. Many chemisorption events require that a detectable activation barrier be overcome, a process known as “activated chemisorption.” Both activated and non-activated chemisorption can involve the intermediacy of physisorbed precursor species, which represent local minima on the potential energy surface<sup>14-17</sup>. Evidence for precursor-mediated adsorption often relies on advanced spectroscopic or molecular beam experiments<sup>18-19</sup>, and the validity of adsorption pathways involving precursors has at times spurred considerable debate<sup>20-21</sup>.

Certain zeolites and metal–organic frameworks feature coordinatively-unsaturated metal cations that can act as strong adsorption sites for various guest species, although the typically electron-poor nature of these sites tends to favor physical, rather than chemical, adsorption processes<sup>1-4</sup>. There has, however, been a growing interest in the synthesis of porous materials bearing electron-rich metal sites primed to engage in covalent interactions with small molecule adsorbates<sup>5-9</sup>. While such adsorbents may engender more exothermic adsorption and therefore higher uptake capacities, chemisorption can also give rise to transport-independent activation barriers akin to those often observed on surfaces<sup>14-15</sup>. Understanding the kinetic profile for chemisorptive events within porous media is critical toward the design and engineering of adsorptive storage and separation processes, and the presence of even modest activation barriers may become problematic for applications that require loading or operation at low temperatures.

To address the lack of studies examining chemisorption kinetics at open metal sites in porous solids, we have investigated the mechanism of H<sub>2</sub> adsorption at the trigonal pyramidal Cu<sup>+</sup> sites within the metal–organic framework Cu<sub>x</sub>Zn<sub>5-x</sub>Cl<sub>4-x</sub>(btdd)<sub>3</sub> (Cu<sup>I</sup>-MFU-4l; H<sub>2</sub>btdd = bis(1*H*-1,2,3-triazolo[4,5-*b*],[4',5'-*i*])dibenzo[1,4]dioxin), which have previously been shown to engage in  $\pi$ -backbonding with H<sub>2</sub> and other  $\pi$ -acidic adsorbates<sup>13</sup>. Herein, we demonstrate that chemisorption of H<sub>2</sub> at these sites occurs through a physisorbed precursor intermediate, which is observable via powder neutron diffraction, representing the first structural characterization of a

precursor species in a chemisorption process. Temperature-programmed desorption and adsorption kinetics measurements are used to confirm the presence of this species and estimate the chemisorption activation barrier, respectively. Computational analysis further reveals that activation of H<sub>2</sub> is associated with a local distortion of the Cu<sup>+</sup> coordination environment that augments its  $\pi$ -backbonding capability. Together, these results holistically demonstrate precursor-mediated adsorption in a porous material.

### ***In situ* Powder Neutron Diffraction Measurements**

The cubic metal–organic framework Zn<sub>5</sub>Cl<sub>4</sub>(btdd)<sub>3</sub> (MFU-4l) is comprised of pentanuclear zinc nodes bridged by bis-triazolate btdd<sup>2-</sup> ligands<sup>22</sup>. Approximately half of its [ZnCl]<sup>+</sup> units can undergo post-synthetic cation exchange to install three-coordinate Cu<sup>+</sup> centers<sup>11</sup> that evoke the trigonal coordination geometries often seen in cuprous zeolites<sup>23,24</sup>. Previous work determined that this material exhibits an isosteric heat of H<sub>2</sub> adsorption of –32 kJ/mol, which is the most exothermic value known for molecular H<sub>2</sub> binding in any metal–organic framework to date<sup>11</sup>. We determined the crystal structure of the evacuated Cu<sup>I</sup>-MFU-4l framework at 7 K using powder neutron diffraction (Fig. 1a-b and Supplementary Fig. 1), and the relative occupancies of the exchangeable metal sites were assigned as 55% Cu and 45% Zn based on the Cu:Zn ratio determined by inductively coupled plasma optical emission spectroscopy (ICP-OES) analysis. In all crystallographic refinements, the copper sites were modeled as three-coordinate Cu<sup>+</sup> centers, while the tetrahedral Zn<sup>2+</sup> centers were capped by a chloro ligand, giving an overall chemical formula of Cu<sub>2.2</sub>Zn<sub>2.8</sub>Cl<sub>1.8</sub>(btdd)<sub>3</sub><sup>25</sup>.

Powder samples of Cu<sup>I</sup>-MFU-4l were dosed with 0.75 D<sub>2</sub> molecules per Cu at 40 K and then cooled to 7 K for neutron diffraction data collection (Supplementary Fig. 2). In the resulting structure, D<sub>2</sub> was located ~1.6 Å from the unsaturated Cu<sup>+</sup> centers (site I, Fig. 1c), indicating very strong binding. This value is also consistent with the Cu–H<sub>2</sub> distance of 1.7 Å calculated previously for the material using density functional theory (DFT)<sup>26</sup>, but the occupancy of the site is only 0.087(18) D<sub>2</sub> molecules per Cu and thus represents a small fraction of the total adsorbed hydrogen (Table 1). The highest occupancy site (site II) is located at the windows of the pentanuclear tetrahedral nodes. Site II is characterized by weak physisorption and likely serves as the primary adsorption site in the parent MFU-4l material, for which the isosteric heat of H<sub>2</sub> adsorption was measured to be –5 kJ/mol at low coverage<sup>22</sup>. One additional site (site I\*) is also occupied under these conditions, located directly above site I and ~3 Å away from the strongly adsorbing Cu<sup>+</sup> centers. Importantly, despite the difficulties posed by compositional disorder of Cu<sup>+</sup> and [Zn–Cl]<sup>+</sup> in this system, refinements strongly suggest that density is present at this position only following D<sub>2</sub> dosing. However, the compositional disorder conspires with powder averaging to obfuscate the occupancy of D<sub>2</sub> at site I\*. Indeed, the occupancy of this site was found to be particularly sensitive to the thermal parameters employed, consistent with a significant degree of D<sub>2</sub> disorder or dynamics. Owing to additional compositional disorder at the metal sites, we modeled the thermal parameters of D<sub>2</sub> at site I\* conservatively, so as to not overestimate its contribution to the total amount of adsorbed D<sub>2</sub> (Supplementary Table 1).

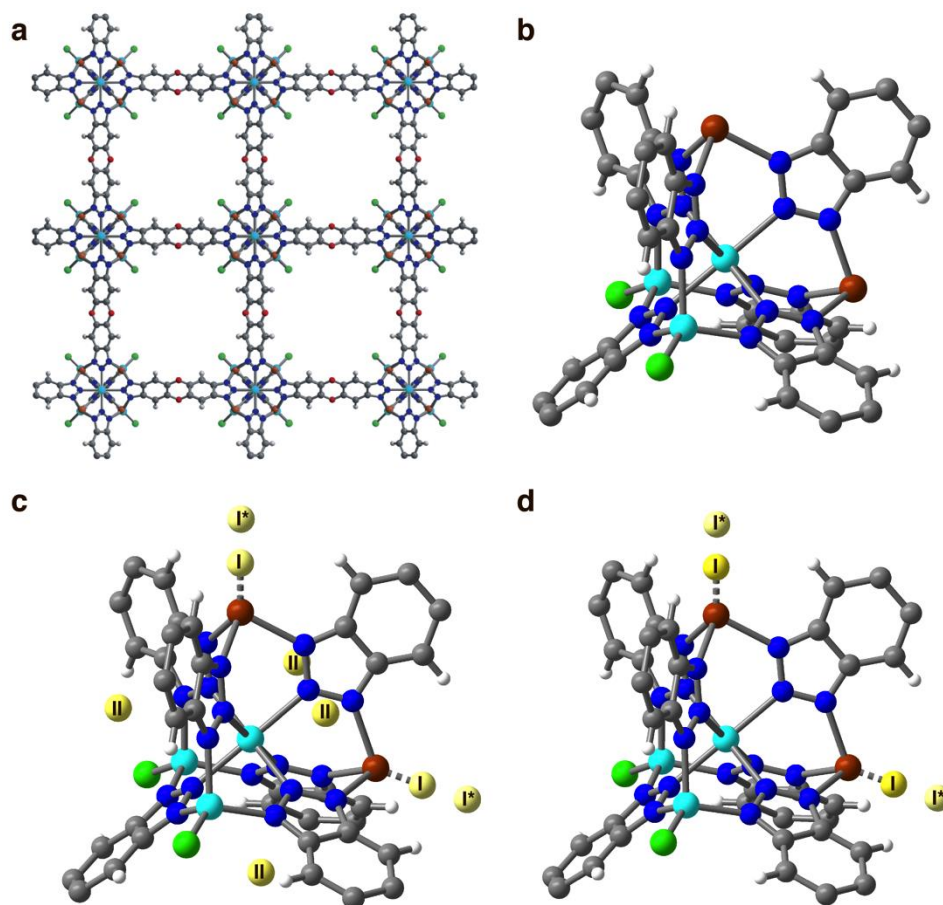


**Fig. 1** Crystal structures of evacuated and  $D_2$ -dosed  $Cu^I$ -MFU-4l. **a**, A portion of the structure of activated  $Cu^I$ -MFU-4l, as determined from powder neutron diffraction data. **b**, Expanded view of the pentanuclear nodes comprising the secondary building units of the framework. **c**, Structure of  $Cu^I$ -MFU-4l obtained at 7 K after dosing with 0.75  $D_2$  molecules per Cu at 40 K and cooling to 7 K. **d**, Structure obtained at 7 K following dosing with 0.75  $D_2$  molecules per Cu at 77 or 300 K. Cyan, brown, green, blue, green, grey, and white spheres represent Zn, Cu, Cl, N, C, and H atoms, respectively; yellow spheres represent isotropically refined  $D_2$  molecules<sup>28-30</sup>.

The separation between sites I and I\* is approximately 30% of the nearest neighbor  $D_2 \cdots D_2$  separation in solid  $D_2$ <sup>27</sup>, and thus it is clear that both sites cannot be occupied simultaneously at a single  $Cu^+$  center. Instead, this proximity suggests an activation barrier to  $D_2$  binding at site I, with site I\* representing a metastable physisorbed state that serves as a precursor to chemisorption. To further investigate this idea, a sample of activated  $Cu^I$ -MFU-4l was dosed with 0.75  $D_2$  molecules per Cu at successively higher temperatures (Supplementary Fig. 3-4). Following dosing at 77 K and subsequent cooling to 7 K,  $D_2$  was found to occupy sites I and I\* exclusively (Fig. 1 and table S1). Importantly, the occupancy of site I is much larger here than when dosed at 40 K, yet it remains significantly lower than 0.75  $D_2$  molecules per Cu. Increasing the dosing temperature to 300 K yields a further increase in the occupancy of site I. The

increasing occupancy of site I with dosing temperature is strongly correlated with an isotropic framework contraction as shown by the decreasing value of cubic lattice parameter  $a$  (Table 1).

**Table 1. Occupancies of D<sub>2</sub> at site I and cubic lattice parameter  $a$ , determined from powder neutron diffraction data obtained after dosing the evacuated framework with 0.75 equivalents of D<sub>2</sub> per Cu at the specified temperature.<sup>a</sup>**

Dosing Temperature (K)	Site I Occupancy	$a$ (Å)
40	0.087(18)	31.2174(10)
77	0.350(18)	31.1652(10)
300	0.513(14)	31.1505(6)

<sup>a</sup>All diffraction data were collected at 7 K, and the super-atom approach was used to model D<sub>2</sub> molecules as isotropic D atoms<sup>28-30</sup>. Occupancies are expressed as molecular equivalents of D<sub>2</sub> per Cu. The value of  $a$  for the evacuated framework at 7 K is 31.2744(14) Å.

Binding of H<sub>2</sub> at site I\* can be described as a physisorbed precursor state, representing a local minimum on the potential energy surface of adsorption<sup>16,17,19,21</sup>. While surface science often relies on spectroscopic or molecular beam experiments to provide indirect evidence for precursor-mediated adsorption<sup>18,19</sup>, the spatial separation of Cu<sup>+</sup> centers in Cu<sup>I</sup>-MFU-4l allows for the trapping and direct observation of this metastable precursor state at low temperatures. Accordingly, the kinetic nature of hydrogen adsorption at the Cu<sup>+</sup> sites in Cu<sup>I</sup>-MFU-4l is more reminiscent of chemisorption on metallic surfaces than of the classical, barrierless physisorption generally observed within porous solids. To our knowledge, this is the first demonstration of a precursor-mediated adsorption within a porous solid.

### Temperature-Programmed Desorption and Kinetics Measurements

Given the compositional disorder inherent to Cu<sup>I</sup>-MFU-4l, we sought to experimentally probe H<sub>2</sub> sorption at Cu<sup>+</sup> in a site-specific manner. Temperature-programmed desorption (TPD) was identified as a promising technique, given the much higher temperature required for H<sub>2</sub> desorption from Cu<sup>+</sup> compared to other sites in the framework<sup>26</sup>. Accordingly, a powder sample of Cu<sup>I</sup>-MFU-4l was first dosed with a known molar quantity of H<sub>2</sub> (substoichiometric with respect to Cu<sup>+</sup>). For samples dosed at 293 K, the sample cell was subsequently cooled to a base temperature of 20 K prior to heating and data collection. A single high-temperature desorption feature ( $T_{\max} = 244$  K) is present following H<sub>2</sub> loading at 293 K (Fig. 2 and Supplementary Fig. 7-9)<sup>26</sup>. In contrast, for samples that are cold-loaded with H<sub>2</sub> at 20 K, a new desorption peak becomes evident at a moderately lower temperature ( $T_{\max} = 216$  K). This temperature is far too high to arise from desorption of H<sub>2</sub> that is not bound to a metal site (*e.g.* from crystallographic site II), as any hydrogen at such sites desorbs below 100 K (see Supplementary Fig. 7 and Ref. 26), but is very much consistent with desorption of H<sub>2</sub> from the crystallographically located precursor site at Cu<sup>+</sup> (I\*). In agreement with the neutron diffraction results, TPD indicates that low-temperature dosing inhibits chemisorption and allows for trapping of some H<sub>2</sub> at the precursor site. However, desorption from the precursor site requires temperatures that are sufficiently high to overcome the chemisorption activation barrier, and accordingly some chemisorption does take place during the heating phase of the TPD experiment. These competing

phenomena result in desorption peaks for both sites at  $\text{Cu}^+$  being present for cold-loaded samples.

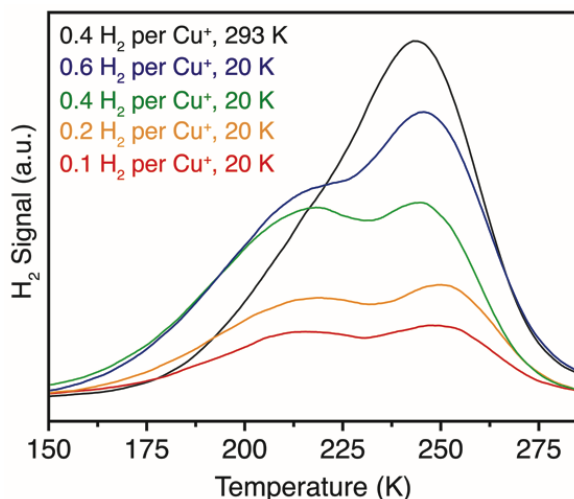


**Fig. 2 Temperature-programmed  $\text{H}_2$  desorption data.** Thermal desorption data obtained for Cu-MFU-4l after loading with  $\text{H}_2$  at 293 or 20 K. The desorption data obtained following loading at 20 K feature a second, lower-temperature peak that can be assigned to desorption of  $\text{H}_2$  directly from the physisorbed precursor state.

Adsorption kinetics experiments were performed to quantitatively assess the activation barrier to access site I from the physisorbed precursor state. The transient adsorption data were fit to a Langmuir first-order rate law<sup>31</sup>, which yielded an activation energy  $E_a = 12.7$  kJ/mol (Supplementary Fig. 10-11). This treatment relies on the approximation that all quantified adsorption occurs at chemisorption site I, and accordingly this value of  $E_a$  is most reasonably taken as a lower bound to the barrier guarding access to site I from precursor site I\*. Importantly, this  $E_a$  value is an order of magnitude larger than the barrier to  $\text{H}_2$  diffusion anticipated within this large-pore framework material<sup>32</sup>, and therefore the kinetics data are reflective of a transport-independent activation barrier. The measured  $E_a$  is also too large to arise from a pathway involving  $\text{H}_2$  desorption from site II and subsequent non-activated chemisorption at site I, for which the activation barrier would be equal in magnitude to the enthalpy of adsorption at site II ( $-5$  kJ/mol)<sup>14</sup>. Accordingly, both TPD and adsorption kinetics further substantiate the role of a precursor intermediate to hydrogen chemisorption at  $\text{Cu}^+$ , and provide support for the legitimacy of adsorption site I\* in the structural model constructed from neutron diffraction data.

### Density Functional Theory Calculations

In order to assess further the structural and electronic changes that occur upon chemisorption of  $\text{H}_2$  at  $\text{Cu}^+$ , we performed DFT calculations on a pentanuclear cluster model that represents a single framework node (Supplementary Fig. 12-14). Binding of hydrogen to  $\text{Cu}^+$  was found to be associated with a decrease in the average framework  $\text{Zn}(O_h)\text{-N}$  distance, which can reasonably be assumed as the cause of the isotropic framework contraction, given that the octahedral  $\text{Zn}^{2+}$

site represents the geometric center of the framework building unit. In addition, the calculations indicate that H<sub>2</sub> binding results in Cu<sup>+</sup> moving away from the octahedral Zn<sup>2+</sup> site by ~0.25 Å (Fig. 3a and Supplementary Fig. 15), resulting in an increased pyramidalization of the Cu<sup>+</sup> coordination sphere. This change in turn destabilizes the degenerate d<sub>π</sub> orbitals (*e* in C<sub>3v</sub> symmetry) that are of proper symmetry to form the π component of the Cu–H<sub>2</sub> interaction (Fig. 3b). Accordingly, Cu<sup>+</sup> migration appears to facilitate enhanced π-backdonation to H<sub>2</sub>. Support for this argument is found via an energy decomposition analysis<sup>33</sup> of the absolutely localized molecular orbitals corresponding to the Cu–H<sub>2</sub> bonding interaction (Supplementary Table 2). For a cluster with all coordinates fully relaxed, Cu→H<sub>2</sub> backdonation contributes –24.4 kJ/mol to the total interaction energy, which is larger than the H<sub>2</sub>→Cu forward donation contribution of –21.7 kJ/mol. However, for a cluster wherein only the H<sub>2</sub> coordinates are allowed to relax while binding to the bare cluster (*i.e.* no migration of Cu<sup>+</sup> occurs), this analysis predicts much weaker backdonation (–11.9 kJ/mol), while forward donation decreases more modestly to –15.8 kJ/mol. Accordingly, these results illuminate an intricate relationship between local structural effects contributing to Cu–H<sub>2</sub> π-backbonding and the contraction of the larger three-dimensional framework.

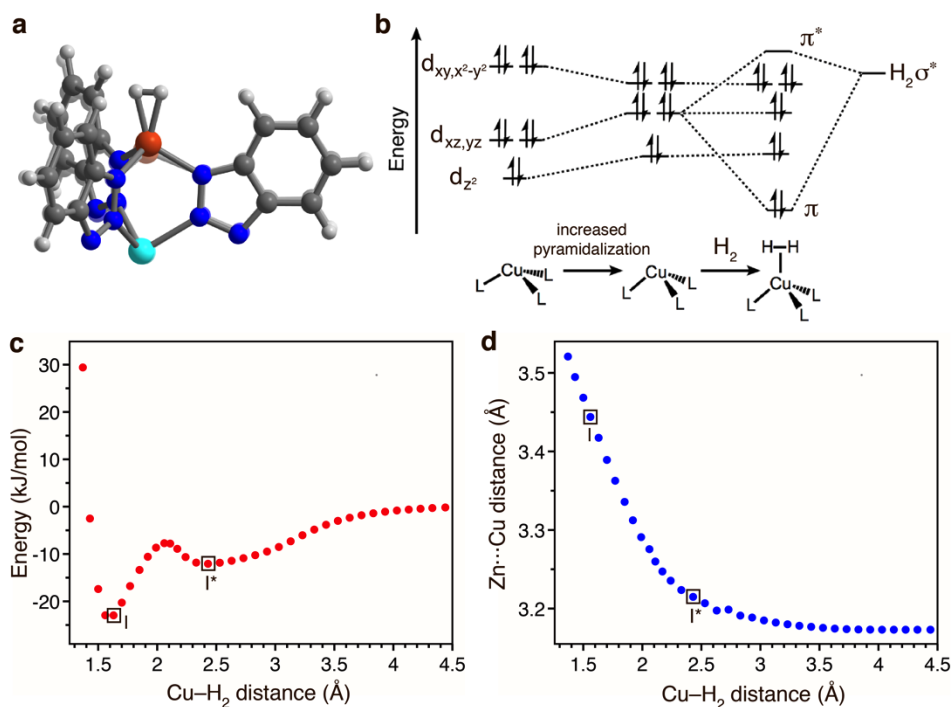


**Fig. 3 Structural and electronic changes associated with H<sub>2</sub> binding in Cu<sup>I</sup>-MFU-4l.** **a**, A portion of the DFT-optimized cluster model, with (solid structure) and without (faded structure) H<sub>2</sub> bound to Cu<sup>+</sup>. **b**, Qualitative molecular orbital energy diagram illustrating how the Cu 3d orbitals are affected by pyramidalization and π-backbonding to H<sub>2</sub>. Interactions between Cu<sup>+</sup> and H<sub>2</sub> of σ symmetry are omitted for clarity. **c**, Calculated potential energy surface along the Cu–H<sub>2</sub> coordinate at the B3LYP-D2/6-31++G\*\*(6-31G\*) level of DFT. **d**, Calculated relationship between the Zn···Cu distance and Cu–H<sub>2</sub> distance at the B3LYP-D2/6-31++G\*\*(6-31G\*) level of DFT.

A scan of the potential energy surface (PES) along the Cu–H<sub>2</sub> coordinate revealed a local minimum corresponding to a physisorbed precursor (Fig. 3c), albeit under rather specific basis set conditions. At the B3LYP-D2/6-31++G\*\*(6-31G\*) level of theory, the optimized structure of the species corresponding to this local minimum shows H<sub>2</sub> bound end-on (Supplementary Fig. 16) with a Cu–H<sub>2</sub>(centroid) distance of 2.43 Å (Fig. 3c). Importantly, the central Zn···Cu distance in this structure is nearly unchanged from that without H<sub>2</sub> present. As shown in Fig. 3d, Cu<sup>+</sup> migration occurs at increasingly shorter Cu–H<sub>2</sub> distances, with the potential energy saddle point occurring at Zn···Cu distance of 2.28 Å, corresponding to a Cu–H<sub>2</sub> separation of 2.06 Å. The calculated barrier separating the shallow well of this local minimum structure from that of the chemisorbed species is 4.4 kJ/mol, which is smaller than the lower bound of 12.7 kJ/mol measured experimentally via adsorption kinetics. Analogous scans of the PES using the def2-TZVPPD(def2-SVP) basis set yield only a shoulder, rather than a true minimum, at Cu–H<sub>2</sub>(centroid) distances between 2 and 3 Å (Supplementary Fig. 17). The difficulties in quantitatively modeling the kinetic pathway of H<sub>2</sub> chemisorption can likely be traced to the increased flexibility available to a single cluster node relative to the extended lattice. Unfortunately, calculation of the PES using a larger computational model that mimics the extended lattice would not be tractable with the modern range separated hybrid functionals employed here. Nevertheless, it is notable that qualitative evidence for precursor-mediated chemisorption can be garnered through analysis of a single cluster node, and these data suggest that the experimental kinetic pathway arises from both local and long-range structural effects.

### Spectroscopic evidence for $\pi$ -backbonding upon H<sub>2</sub> binding

X-ray absorption spectroscopy (XAS) data were collected at the Cu L-edge for evacuated and H<sub>2</sub>-dosed samples of Cu<sup>I</sup>-MFU-4l to investigate experimentally the electronic character of the Cu<sup>+</sup>–H<sub>2</sub> interaction upon chemisorption. Importantly, XAS serves as an excellent probe of electronic perturbations of the valence d manifold<sup>34</sup>. The spectrum for activated Cu<sup>I</sup>-MFU-4l displays L<sub>3</sub> and L<sub>2</sub> edge features at 936 and 956 eV, respectively (Fig. 4a)<sup>35</sup>. Given the absence of a pure 3d hole for electron excitation, these transitions arise due to mixing of Cu 3d character into vacant orbitals of largely  $\sigma^*$  character<sup>36</sup>. Following *in situ* H<sub>2</sub> dosing at 25 °C, the L<sub>3</sub> and L<sub>2</sub> edge features shift to lower energies by approximately 0.5 and 0.7 eV, respectively, and grow in intensity with increasing H<sub>2</sub> pressure from 200 to 1000 mbar. Based on complementary H<sub>2</sub> adsorption isotherm data (Supplementary Fig. 18), only partial coverage of the Cu<sup>+</sup> sites with H<sub>2</sub> is achieved under these conditions, and thus the edges consist of superimposed peaks from coordinatively-unsaturated and H<sub>2</sub>-bound Cu<sup>+</sup> centers. Nevertheless, the increase in edge intensity with H<sub>2</sub> dosing can be directly traced to increased metal-to-ligand charge transfer via  $\pi$ -backdonation<sup>34,35,37</sup>.

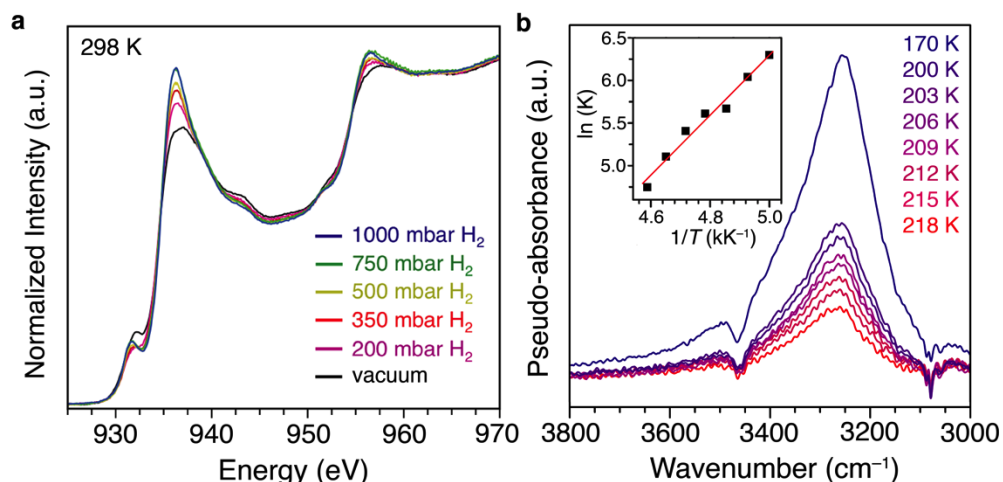


**Fig. 4 Spectroscopic evidence of  $\pi$ -backbonding.** **a**, *In situ* Cu L-edge X-ray absorption spectra for evacuated Cu<sup>I</sup>-MFU-4l (black) and after dosing with various pressures of H<sub>2</sub> at 25 °C. **b**, Fundamental  $\nu(\text{H-H})$  vibration at a constant H<sub>2</sub> loading at different temperatures, with the inset showing the corresponding van't Hoff plot and linear regression used to determine  $\Delta H^\circ_{\text{ads}}$  and  $\Delta S^\circ_{\text{ads}}$ .

For physisorbed H<sub>2</sub>, the vibrational energy of the fundamental  $\nu(\text{H-H})$  band is generally modestly red-shifted relative to that of the free molecule (4050–4150 versus 4161 cm<sup>-1</sup>)<sup>38,39</sup>. In contrast, the *in situ* DRIFTS spectrum of Cu<sup>I</sup>-MFU-4l dosed with H<sub>2</sub> exhibits a broad feature of weak intensity centered at 3252 cm<sup>-1</sup>, corresponding to the fundamental  $\nu(\text{H-H})$  stretch (Fig. 4b)<sup>40</sup>. Using the spectrum for the D<sub>2</sub>-dosed material as a baseline, we were able to isolate this band from framework vibrations and obtain a difference spectrum with peaks associated only with chemisorbed H<sub>2</sub> or D<sub>2</sub> (Supplementary Fig. 19). Unlike most molecular Kubas complexes<sup>41</sup>, Cu<sup>I</sup>-MFU-4l offers a unique opportunity to study the thermodynamics of H<sub>2</sub> binding to a low-valent metal site directly and without consideration of a prior ligand dissociation step. To this end, variable-temperature DRIFTS data were collected for a sample of the H<sub>2</sub>-dosed framework between 200 and 218 K (Fig. 4b). Integration of the corresponding  $\nu(\text{H-H})$  peak enabled calculation of the fractional coverage by comparison to the peak area under saturation conditions (170 K)<sup>42,43</sup>. A van't Hoff analysis afforded an enthalpy value  $\Delta H^\circ_{\text{ads}} = -28(2)$  kJ/mol and entropy value  $\Delta S^\circ_{\text{ads}} = -89(8)$  J/(mol·K). These values are in good agreement with the thermodynamic parameters calculated from DFT (Supplementary Table 3) and with the isosteric heat of adsorption measured previously from gas adsorption data<sup>13</sup>.

## Outlook

The soft, electron-rich Cu<sup>+</sup> sites present in Cu<sup>I</sup>-MFU-4l serve as a counterpoint to the hard, Lewis acidic open metal sites accessible in many metal–organic frameworks and zeolites, and their aptitude for  $\pi$ -backbonding leads to non-dissociative hydrogen binding via chemisorption. The resulting large magnitude of  $\Delta H^\circ_{\text{ads}}$  renders this framework an intriguing candidate for adsorptive hydrogen storage at ambient and even elevated temperatures<sup>12</sup>. However, this study clearly illustrates the kinetic complexities that can be associated with chemisorption in porous materials, and reinforces the importance of analyzing adsorption kinetics in chemisorption-driven processes. We anticipate that physisorbed precursors will be realized as relevant

intermediates in other chemisorption processes within porous solids, and hope this work provides a roadmap for designing experiments that will enable their identification.

### References and Notes:

1. Kulprathipanja, S., Ed. *Zeolites in industrial separation and catalysis*. 1<sup>st</sup> Ed. (Wiley-VCH Verlag GmbH & Co. KGaA, Weinheim, 2010).
2. Li, J.-R., Kuppler, R. J. & Zhou, H.-C. *Chem. Soc. Rev.* **38**, 1477–1504 (2009).
3. Dincă, M. & Long, J. R. Hydrogen storage in microporous metal–organic frameworks with exposed metal sites. *Angew. Chem. Int. Ed.* **47**, 6766–6779 (2008).
4. Yaghi, O. M., Kalmutzki, M. J. & Diercks, C. S. *Introduction to reticular chemistry: Metal–organic frameworks and covalent organic frameworks* (Wiley-VCH Verlag & Co. KGaA, Weinheim, 2019).
5. Bloch, E. D. *et al.* Selective binding of O<sub>2</sub> over N<sub>2</sub> in a redox-active metal–organic framework with open iron(II) coordination sites. *J. Am. Chem. Soc.* **133**, 14814–14822 (2011).
6. Anderson, J. S., Gallagher, A. T., Mason, J. A. & Harris, T. D. *J. Am. Chem. Soc.* **136**, 16489–16492 (2014).
7. Reed, D. A. *et al.* A spin transition mechanism for cooperative adsorption in metal–organic frameworks. *Nature* **274**, 96–100 (2017).
8. Zhang, J.-P. & Kitagawa, S. Supramolecular isomerism, framework flexibility, unsaturated metal center, and porous property of Ag(I)/Cu(I) 3,3',5,5'-tetramethyl-4,4'-bipyrazolate. *J. Am. Chem. Soc.* **130**, 907–917 (2008).
9. Burgun, A. *et al.* Mapping-out catalytic processes in a metal–organic framework with single-crystal X-ray crystallography. *Angew. Chem. Int. Ed.* **56**, 8412–8416 (2017).
10. Sato, H. *et al.* Self-accelerating CO sorption in a soft nanoporous crystal. *Science* **343**, 167–170 (2014).
11. Lee, K. *et al.* Design of a metal–organic framework with enhanced back bonding for separation of N<sub>2</sub> and CH<sub>4</sub>. *J. Am. Chem. Soc.* **136**, 698–704 (2014).
12. Allendorf, M. D. *et al.* An assessment of strategies for the development of solid-state adsorbents for vehicular hydrogen storage. *Energy Environ. Sci.* **11**, 2784–2812 (2018).
13. Denysenko, D., Grzywa, M., Jelic, J., Reuter, K. & Volkmer, D. Scorpionate-type coordination in MFU-4l metal–organic frameworks: Small-molecule binding and activation upon the thermally activated formation of open metal sites. *Angew. Chem. Int.*

- Ed.* **53**, 5832–5836 (2014).
14. Masel, R. I. *Principles of adsorption and reaction on solid surfaces* (John Wiley & Sons, Inc., New York, NY, 1996).
  15. Kolasinski, K. W. *Surface science: Foundations of catalysis and nanoscience* (John Wiley & Sons, Inc., Hoboken, NJ, Ed. 2, 2008).
  16. Bowker, M. The role of precursor states in adsorption, surface reactions and catalysis. *Top. Catal.* **59**, 663–670 (2016).
  17. Brown, D. E., Moffatt, D. J. & Wolkow, R. A. Isolation of an intrinsic precursor to molecular chemisorption. *Science* **279**, 542–544 (1998).
  18. Rendulic, K. D. & Winkler, A. Adsorption and desorption dynamics as seen through molecular beam techniques. *Surface Sci.* **299–300**, 261–276 (1994).
  19. Beutl, M., Rendulic, K. D. & Castro, G. R. Does the rotational state of a molecule influence trapping in a precursor? An investigation of N<sub>2</sub>/W(100), CO/FeSi(100) and O<sub>2</sub>/Ni(111). *Surface Sci.* **385**, 97–106 (1997).
  20. Grunze, M. & Kreuzer, H. J., Eds., *Kinetics of interface reactions* (Springer-Verlag, Berlin, 1986), Vol. 8.
  21. Beutl, M. *et al.* There is a true precursor for hydrogen adsorption after all: the system H<sub>2</sub>/Pd(111) + subsurface V. *Chem. Phys. Lett.* **342**, 473–478 (2001).
  22. Denysenko D. *et al.*, Elucidating gating effects for hydrogen sorption in MFU-4-type triazolate-based metal-organic frameworks featuring different pore sizes. *Chem. Eur. J.* **17**, 1837–1848 (2011).
  23. Fowkes, A. J., Ibberson, R. M. & Rosseinsky, M. J. Structural characterization of the redox behavior in copper-exchanged sodium zeolite Y by high-resolution powder neutron diffraction. *Chem. Mater.* **14**, 590–602 (2002).
  24. Ipek, B., Pollock, R. A., Brown, C. M., Uner, D. & Lobo, R. F. H<sub>2</sub> adsorption on Cu(I)-SSZ-13. *J. Phys. Chem. C* **122**, 540–548 (2018).
  25. For more on our choice of crystallographic model, see the Supplementary Information.
  26. Weinrauch, I. *et al.*, Capture of heavy hydrogen isotopes in a metal-organic framework with active Cu(I) sites. *Nat. Commun.* **8**, 14496 (2017).
  27. Van Kranendonk, J. & Gush, H. P. The crystal structure of solid hydrogen. *Phys. Lett.* **1**, 22–23 (1962).

28. Pollock, R. A., Her, J.-H., Brown, C. M., Liu, Y. & Dailly, A. Kinetic trapping of D<sub>2</sub> in MIL-53(Al) observed using neutron scattering. *J. Phys. Chem. C* **118**, 18197–18206 (2014).
29. Wu, H., Zhou, W. & Yildirim, T. Hydrogen storage in a prototypical zeolitic imidazolate framework-8. *J. Am. Chem. Soc.* **129**, 5314–5315 (2007).
30. Brown, C. M., Liu, Y., Yildirim, T., Peterson, V. K. & Kepert, C. J. Hydrogen adsorption in HKUST-1: a combined inelastic neutron scattering and first-principles study. *Nanotechnology* **20**, 204025 (2009).
31. Liu, Y. & Shen, L. From Langmuir kinetics to first- and second-order rate equations for adsorption. *Langmuir* **24**, 11625–11630 (2008).
32. Saha, D., Wei, Z. & Deng, S. Hydrogen adsorption equilibrium and kinetics in metal–organic framework (MOF-5) synthesized with DEF approach. *Sep. Purif. Technol.* **64**, 280–287 (2009).
33. Khaliullin, R. Z., Cobar, E. A., Lochan, R. C., Bell, A. T. & Head-Gordon, M. Unraveling the origin of intermolecular interactions using absolutely localized molecular orbitals. *J. Phys. Chem. A* **111**, 8753–8765 (2007).
34. Hocking, R. K. *et al.* Fe L-Edge XAS studies of K<sub>4</sub>[Fe(CN)<sub>6</sub>] and K<sub>3</sub>[Fe(CN)<sub>6</sub>]: A direct probe of back-bonding. *J. Am. Chem. Soc.* **128**, 10442–10451 (2006).
35. Su, G. M. *et al.* Backbonding contributions to small molecule chemisorption in a metal–organic framework with open copper(I) centers. Submitted.
36. Harkins, S. B., Mankad, N. P., Miller, A. J. M., Szilagyi, R. K. & Peters, J. C. Probing the electronic structures of [Cu<sub>2</sub>(μ-XR<sub>2</sub>)]<sup>n+</sup> diamond cores as a function of the bridging X atom (X = N or P) and charge (n = 0, 1, 2). *J. Am. Chem. Soc.* **130**, 3478–3485 (2008).
37. George, S. J., Lowery, M. D., Solomon, E. I., Cramer, S. P. Copper L-edge spectral studies: A direct experimental probe of the ground-state covalency in the blue copper site in plastocyanin. *J. Am. Chem. Soc.* **115**, 2968–2969 (1993).
38. Vitillo, J. G. *et al.* Role of exposed metal sites in hydrogen storage in MOFs. *J. Am. Chem. Soc.* **130**, 8386–8396 (2008).
39. M. T. Kapelewski *et al.*, M<sub>2</sub>(m-dobdc) (M = Mg, Mn, Fe, Co, Ni) Metal–organic frameworks exhibiting increased charge density and enhanced H<sub>2</sub> binding at the open metal sites. *J. Am. Chem. Soc.* **136**, 12119–12129 (2014).
40. FitzGerald, S. A., Mukasa, D., Rigdon, K. H., Zhang, N. & Barnett, B. R. Hydrogen isotope separation within the metal–organic framework Cu(I)-MFU-4l. *J. Phys. Chem. C*.

123, 30427–30433 (2019).

41. Kubas, G. J. *Metal dihydrogen and  $\sigma$ -bond complexes: Structure, theory and reactivity* (Kluwer Academic/Plenum Publishers, New York, NY, 2001).
42. Garrone, E. & Otero Areán, C. Variable temperature infrared spectroscopy: A convenient tool for studying the thermodynamics of weak solid–gas interactions. *Chem. Soc. Rev.* **34**, 846 (2005).
43. FitzGerald, S. A. *et al.* Metal-specific interactions of H<sub>2</sub> adsorbed within isostructural metal–organic frameworks. *J. Am. Chem. Soc.* **133**, 20310–20318 (2011).

## Methods

**General synthesis and characterization methods.** Unless otherwise stated, reagent-grade starting materials were purchased from commercial sources and either used as received or purified by standard procedures<sup>44</sup>. Solvents were sparged with Ar, dried over activated 3 Å molecular sieves, and stored in a glovebox prior to use. The framework MFU-4l was prepared as described previously<sup>22</sup>. Elemental analyses were performed in the Microanalytical Laboratory at the University of California, Berkeley. Inductively-coupled plasma–optical emission spectroscopy (ICP-OES) measurements were performed on an Optima 7000 DV instrument that is maintained by the Microanalytical Laboratory. Metal–organic framework samples (1–3 mg) analyzed by ICP-OES were digested in a small amount (< 1 mL) of concentrated nitric acid, and then diluted in Milli-Q ultrapure water to a concentration of 1–10 ppm Zn and Cu.

**Synthesis of Cu<sup>I</sup>-MFU-4l.** The framework Cu<sup>I</sup>-MFU-4l was synthesized using a procedure adapted from the literature<sup>13,40</sup>. In an N<sub>2</sub>-filled glovebox, a *N,N*-dimethylacetamide (DMA) solution of CuCl<sub>2</sub> (0.275 g, 2.05 mmol, 20 equiv., 20 mL) was added to activated MFU-4l (0.125 g, 0.100 mmol) in a 20 mL borosilicate vial. The vial was capped, placed in a hotplate well, and heated to 60 °C for 20 h. The mother liquor was subsequently decanted, and the sample was soaked in fresh DMA at 60 °C for 12 h. This process was repeated one additional time. After this second soaking, the DMA was decanted, and the framework was soaked in MeOH at 60 °C. The mother liquor was decanted and replaced with fresh MeOH three times over the course of two days (total of four MeOH washes). The resulting green solid was dried *in vacuo* at 60 °C in the glovebox, during which time it slowly became brown in color. The vial was then sealed and transferred to a wet, O<sub>2</sub>-free glovebox filled with a Praxair Hydrostar<sup>®</sup> (5% H<sub>2</sub> in N<sub>2</sub>) gas mixture (*note*: the H<sub>2</sub> atmosphere is not necessary for this synthetic protocol). To the framework was added a MeOH solution of lithium formate hydrate (0.400 g, 5.71 mmol, 20 mL). The mixture was allowed to stand at room temperature for 1 h. The mother liquor was then decanted, and the framework was soaked in fresh MeOH at room temperature. This process was repeated four times over the course of 24 h (total of five MeOH washes). The framework was then dried in the glovebox *in vacuo* at 80 °C, yielding Cu<sup>II</sup>-MFU-4l-formate as a light green powder. Autoreduction of the Cu<sup>2+</sup> centers to yield Cu<sup>I</sup>-MFU-4l was accomplished using a Micromeritics ASAP2020 instrument. A sample of Cu<sup>II</sup>-MFU-4l-formate in a glass tube capped with a Transeal was heated *in vacuo* at 100 °C for 12 h, and then ramped at 2 °C/min to 180 °C, where it was

held for 3 h. Between 120–180 °C, extensive offgassing occurs, and the sample changes in color from light green to beige.

**Elemental analysis.** Over multiple batches, metals analysis using ICP-OES gave Cu:Zn ratios of approximately 0.75, consistent with a formula of  $\text{Cu}_{2.2}\text{Zn}_{2.8}\text{X}_n(\text{btdd})_3$  ( $\text{X}^-$  = chloride, formate). Lithium content was consistently found to be below the instrument detection limit. Combustion analysis on activated samples of  $\text{Cu}^{\text{I}}$ -MFU-4l yielded the following CHN percent weights: C, 36.77; H, 1.15; N, 21.08 (average of measurements from three separate batches). For a material with the above metals ratio and a chloride ligand on all of the tetrahedral Zn sites, this would yield a formula of  $\text{C}_{36}\text{H}_{12}\text{N}_{18}\text{O}_6\text{Cu}_{2.2}\text{Zn}_{2.8}\text{Cl}_{1.8}$ , with an expected analysis of: C, 36.66; H, 1.02; N, 21.38. If all of the chlorides were replaced with formate, this would yield a formula of  $\text{C}_{37.8}\text{H}_{13.8}\text{N}_{18}\text{O}_{9.6}\text{Cu}_{2.2}\text{Zn}_{2.8}$ , with an expected analysis of: C, 37.94; H, 1.16; N, 21.07. Given the significant discrepancy between the carbon contents of this latter theoretical value and that measured for our samples (37.94 vs. 36.77, respectively), we proceeded to model the anionic ligands capping the tetrahedral Zn sites as chlorides in our crystallographic model (see below section on powder neutron diffraction).

**Measurement of hydrogen adsorption isotherm data.** UHP-grade (99.999% purity)  $\text{H}_2$  and He were used for all adsorption measurements. Gas adsorption isotherms in the pressure range of 0–1.0 bar were measured using a volumetric method on a Micromeritics 3Flex gas sorption analyzer. Samples of  $\text{Cu}^{\text{I}}$ -MFU-4l were prepared in preweighed analysis tubes capped with a Transeal via autoreduction of  $\text{Cu}^{\text{II}}$ -MFU-4l-formate *in vacuo* at 180 °C (ramp rate = 2 °C/min) until the outgas rate was determined to be less than 2  $\mu\text{bar}/\text{min}$  (approximately 3–4 h). The tube was then weighed and subsequently transferred to the analysis port of the instrument. Free space measurements were performed using He at the analysis temperature. A Julabo F32 water circulator was used as the isothermal bath. Oil-free vacuum pumps and oil-free pressure regulators were used for all measurements to prevent contamination of the samples during evacuation or of the feed gases during isotherm measurements.

**Powder neutron diffraction measurements.** Powder neutron diffraction measurements were performed on 0.362 g  $\text{Cu}^{\text{I}}$ -MFU-4l at the National Institute of Standards and Technology Center for Neutron Research (NCNR). Data was collected at the high-resolution neutron powder diffractometer, BT1, utilizing a Ge(311) monochromator with an in-pile 60' collimator, corresponding to a neutron wavelength of 2.0775 Å. The activated sample was loaded into a vanadium sample can in a He environment glovebox, and sealed with an indium o-ring onto a copper heating block containing a valved outlet for gas loading. After mounting the sample onto a bottom-loaded closed cycle refrigerator (CCR), the sample was cooled to base temperature for measurement. For  $\text{D}_2$  gas dosing, the sample was connected to a fixed-volume gas manifold, heated to  $T = 40, 77, \text{ or } 300$  K, and cooled back to base temperature for measurement of Rietveld quality data collection (~6 to ~8 h per data set), or at the noted temperature for lattice constant determination (~1 h per data set).

Powder neutron diffraction data were analyzed using the GSAS software suite<sup>45,46</sup>. Initial Le Bail refinements were first conducted to determine a background function, lattice parameters, and peak shapes<sup>47</sup>. The peak shape of the bare model was applied to all subsequent refinements for consistency. The position and orientation of the  $\text{btdd}^{2-}$  ligands were refined using restraints to

ensure planarity/bond lengths in line with chemical reasoning. The super-atom approach was used to approximate the D<sub>2</sub> molecule as a single D-atom with double occupancy<sup>28-30</sup>.

An extended discussion on the refinement procedures and construction of structure solutions can be found in the Supplementary Text.

**Temperature-programmed desorption measurements.** TPD measurements utilizing sub-stoichiometric H<sub>2</sub> dosing were performed at Oberlin College. Within an argon-filled glovebox, activated Cu<sup>I</sup>-MFU-4l powder (10-47 mg) was transferred to a cylindrical copper cell. In some cases, the powder was compacted inside the cell by pressing on it with a 1/8<sup>th</sup> inch diameter stainless steel rod. The compacted pellet sample could be returned to a loose powder form using a fine-tipped dental tool. All sample manipulations were performed inside the glovebox before sealing the cell using Swagelok fittings to an ORS2 bonnet valve. The sealed cell was removed from the glovebox and mounted to the base of a modified Janis ST-300T closed-cycle helium cryostat. The sample temperature was determined using a Si-diode thermometer mounted on a copper block attached to the sample cell. The temperature was maintained using a Lakeshore Model 331 controller. A small quantity (less than 0.2 mbar) of He gas was introduced to the system to ensure thermal contact between the sample and the walls of the cell. Gas dosing was performed using a Micromeritics ASAP 2020 instrument. All gases were of research grade (> 99.99% purity). TPD was performed by first exposing the sample to a known amount of H<sub>2</sub> at a desired load temperature (20 or 293 K). The sample was then cooled at 5 K/min to a base temperature of 20 K. At this temperature, virtually all hydrogen was adsorbed. In all cases the sample was maintained at the base temperature for at least 30 min. The sample was then heated at 5 K/min while measuring the evolving gas using a Hiden Analytical “Lo MASS” series quadrupole mass spectrometer. The instrument is optimized for quantifying low mass species and has a base operating pressure of 10<sup>-9</sup> Torr when used in conjunction with a low-pressure capillary orifice.

Temperature programmed desorption (TPD) data utilizing excess H<sub>2</sub> were collected at the National Renewable Energy Laboratory (NREL) using a custom-built apparatus that allows for identification and quantification of effluent gases. Samples may be exposed to hydrogen (99.9999%) at pressures up to 1000 Torr, and the system can achieve pressures as low as 10<sup>-9</sup> Torr. The TPD system is equipped with a mass spectrometer with detection range of 0–100 atomic mass units to detect impurities present in materials both during degas and after hydrogen exposures. In this work, the sample was initially degassed to 423 K, dosed and equilibrated over 0.4 Torr H<sub>2</sub> at either 76 K (the boiling point of nitrogen in Golden, CO) or room temperature. The sample was then cooled with liquid N<sub>2</sub>, evacuated, and upon heating at 15 K/min, the H<sub>2</sub> desorbed was measured.

**Hydrogen adsorption kinetics.** Adsorption kinetics measurements were performed at 276, 279, and 284 K on a Micromeritics 3Flex gas sorption analyzer. A Julabo F32 water circulator was used as the isothermal bath. The manifold pressure and material uptake were monitored as a function of time (0.5 Hz) using the DataMonitor software from Micromeritics. A sample of activated Cu<sup>I</sup>-MFU-4l (0.089 g) was loaded into a glass sample tube capped with a transeal. A glass rod of approximately equal length was inserted so as to minimize the free space within the tube. Free space measurements were performed using He at the analysis temperature. Following complete evacuation of He, the samples were dosed with 2.0 mmol/g of H<sub>2</sub>. The time at which the valve connecting the sample tube to the instrument manifold opened was taken as  $t = 0$  s. The

first two seconds of data were discarded, as control experiments utilizing an empty tube showed that significant pressure changes due solely to gas expansion occurred during this period. When adsorption over the framework sample was monitored, nearly all adsorption was seen to occur within 6 s. Accordingly, the timepoints between 2–6 s were utilized to construct plots of coverage versus time. The transient adsorption data were found to be modeled very well by the first-order Langmuir rate law (also known as the Lagergren expression)<sup>31</sup>:

$$\frac{d\theta_t}{dt} = k_1(\theta_e - \theta_t)$$

in which  $\theta_t$  is the fractional coverage at a given time  $t$ ,  $\theta_e$  is the fractional coverage at equilibrium, and  $k_1$  is the first-order rate constant. Upon integration, this expression becomes:

$$\ln(\theta_e) - \ln(\theta_e - \theta_t) = k_1 t$$

As shown in Supplementary Fig. 10, the transient adsorption data obtained for Cu<sup>I</sup>-MFU-4l conform very well to this expression. Note that inferior fits were obtained using a second-order Langmuir kinetic expression. For an in-depth discussion on the merits of the first- and second-order kinetic expressions, see Ref. 31. The Arrhenius expression was used to calculate an activation barrier  $E_a$ :

$$k_{obs} = Ae^{\frac{-E_a}{RT}}$$

where  $k_{obs}$  is a rate constant measured at temperature  $T$ , and  $A$  is the pre-exponential constant. The rate constants determined for 276, 279, and 284 K adsorption experiments are 0.5389 s<sup>-1</sup> and 0.5713 s<sup>-1</sup>, and 0.6297 s<sup>-1</sup>, respectively. This yields an activation energy  $E_a$  of 12.7 kJ/mol (Supplementary Fig. 11).

**Density Functional Theory calculations.** Calculations were performed using a pentanuclear cluster model that represents the metal–organic framework building unit, where the btdd<sup>2-</sup> ligands have been truncated to benzotriazolates. The central octahedral Zn<sup>2+</sup> is surrounded by four metals in trigonal coordination environments. Two of these metals are Zn<sup>2+</sup> and are capped with a charge-balancing chloride. The other two metal sites are three-coordinate Cu<sup>+</sup> centers. See the supplementary text for an extended description of the methods utilized in the calculations reported herein.

**Cu L-edge X-ray absorption spectroscopy.** Soft X-ray spectroscopy measurements at energies near the Cu L-edge were performed at bending magnet beamline 6.3.2 at the Advanced Light Source, Lawrence Berkeley National Laboratory. H<sub>2</sub> gas dosing experiments made use of a custom-built gas cell and similar apparatus as previously described<sup>48-50</sup>. Samples were deposited on X-ray transparent 150 nm thick, 2.0 mm × 2.0 mm silicon nitride windows supported by a silicon frame (Silson Ltd.). To improve adhesion of the framework to the substrate, polystyrene (M<sub>w</sub> = 350 kg/mol, M<sub>n</sub> = 170 kg/mol) was dissolved in toluene at a concentration of 20 mg/mL and spin coated on top of the silicon nitride windows (2,000 rpm, 40 s) to form a thin polystyrene film (polystyrene exhibits minimal absorption near the Cu L-edge). Pre-activated Cu<sup>I</sup>-MFU-4l was suspended in *n*-hexane in an argon-filled glovebox, sealed in a borosilicate vial, removed

from the glovebox and sonicated for 5 min. The vial was then brought back into the glovebox, and the framework was drop-cast atop the polystyrene-coated Si<sub>3</sub>N<sub>4</sub> windows. After evaporation of the hexane, the window was heated *in vacuo* at 80 °C (approximately 50 mTorr) for at least 2 h. Samples were then sealed in vials and transferred to a N<sub>2</sub>-filled glovebox where they were loaded into the gas cell and sealed before bringing to the beamline. The beamline X-ray energy was calibrated to the edge step of a Cu filter, which was set to 1.3293 nm (932.7 eV). Once attached to the beamline, the sample was pumped and kept at high vacuum ( $\sim 10^{-7}$  Torr) for at least 30 min before any NEXAFS spectra were collected. A transmission NEXAFS spectra of the activated framework was collected before any exposure to H<sub>2</sub> gas. Following collection of NEXAFS spectra of the activated material, H<sub>2</sub> gas (Praxair, Ultra High Purity grade) was slowly introduced in the gas cell and spectra were collected *in situ* at H<sub>2</sub> pressures of 200, 350, 500, 750, and 1000 mbar. After gas dosing, the gas cell was pumped back down to high vacuum and a final spectrum was measured to ensure reversibility. A bare polystyrene-coated silicon nitride window was used for background correction. For normalization, a line was regressed to the pre-edge region and a polynomial regressed to the post-edge region using the Athena software package<sup>51</sup>. The sample position was not moved during measurement to minimize effects due to spatial and thickness inhomogeneity of the drop-cast sample.

**Diffuse reflectance infrared spectroscopy (DRIFTS) measurements.** Infrared spectra were collected using a Bruker Vertex 70 spectrometer equipped with a glowbar source, KBr beamsplitter, and a liquid nitrogen cooled mercury-cadmium-telluride detector. A custom-built diffuse reflectance system with an IR-accessible gas dosing cell was used for all measurements. Sample temperature was controlled by an Oxford Instruments OptistatDry TLEX cryostat, and sample atmosphere was controlled by a Micromeritics ASAP 2020Plus gas sorption analyzer. In a typical experiment, activated framework material was dispersed in dry KBr (10 wt %) in an argon-filled glovebox and evacuated at room temperature overnight. Spectra were collected *in situ* under UHP-grade H<sub>2</sub> and D<sub>2</sub> (99.6 atom % D, Sigma-Aldrich) at 4 cm<sup>-1</sup> resolution continually until equilibrium was observed.

### Data availability

The supplementary information contains additional experimental details on some of the measurements reported herein, as well as supplementary figures and tables. Crystallographic data are available free of charge from the Cambridge Crystallographic Data Centre (CCDC). The CCDC numbers for the powder neutron diffraction structures reported here are 1987754-1987758.

### References

44. Armarego, W. L. F. & Chai, C. L. L. *Purification of Laboratory Chemicals*, (Elsevier, 2003).
45. Larson, A. C. & Von Dreele, R. B. General Structure Analysis System (GSAS), Los Alamos National Laboratory Report LAUR, **2000**, 86–748.
46. Toby, H. B. EXPGUI, a graphical user interface for GSAS. *Appl. Cryst.* **34**, 210–213

(2001).

47. Le Bail, A. Whole powder pattern decomposition methods and applications: A retrospection. *Powder Diffr.* **20**, 316–326 (2005).
48. Drisdell, W. S. & Kortright, J. B. Gas cell for *in situ* soft X-ray transmission-absorption spectroscopy of materials. *Rev. Sci. Instrum.* **85**, 074103 (2014).
49. Drisdell, W. S. *et al.* Probing adsorption interactions in metal–organic frameworks using X-ray spectroscopy. *J. Am. Chem. Soc.* **135**, 18183–18190 (2013).
50. Drisdell, W. S. *et al.* Probing the mechanism of CO<sub>2</sub> capture in diamine-appended metal–organic frameworks using measured and simulated X-ray spectroscopy. *Phys. Chem. Chem. Phys.* **17**, 21448–21457 (2015).
51. Ravel, B. & Newville, M. Athena, Artemis, Hephaestus: Data analysis for X-ray absorption spectroscopy using ifeffit. *J. Synchrotron Radiat.* **12**, 537–541 (2005).

## Acknowledgements

The authors gratefully acknowledge research support from the Hydrogen Materials – Advanced Research Consortium (HyMARC), established as part of the Energy Materials Network under the U.S. Department of Energy, Office of Energy Efficiency and Renewable Energy, Fuel Cell Technologies Office, under Contract Number DE-AC02-05CH11231. X-ray absorption spectroscopy measurements were performed at Beamline 6.3.2 of the Advanced Light Source, Lawrence Berkeley National Laboratory, supported by the Director, Office of Science, Office of Basic Energy Sciences, of the U.S. Department of Energy under Contract DE-AC02-05CH11231. H.A.E and B.A.T. were supported by an NRC/NIST Research Fellowship and a NIST Director’s Postdoctoral Fellowship, respectively. G.M.S. and W.S.D. were supported by the Center for Gas Separations Relevant to Clean Energy Technologies, an Energy Frontier Research Center supported by the U.S. Department of Energy, Office of Science, Office of Basic Energy Sciences, under Award DE-SC0001015. S.A.F. thanks the U.S. National Science Foundation for funding (CHE-1565961). Certain commercial equipment, instruments, or materials are identified in this document. Such identification does not imply recommendation or endorsement by the National Institute of Standards and Technology, nor does it imply that the products identified are necessarily the best available for the purpose. We thank Dr. Katie R. Meihaus for editorial assistance, and Dr. Hiroyasu Furukawa and Dr. T. David Harris for helpful discussions.

## Author contributions

B.R.B. and J.R.L. conceptualized the project and wrote the paper with input from all coauthors. B.R.B. performed all synthetic manipulations and isotherm data collection. H.A.E, B.A.T.,

J.D.T., and C.M.B. collected and analyzed the powder neutron diffraction data. G.M.S. and W.S.D. collected and analyzed the L-edge X-ray absorption spectra. H.Z.H.J. collected and analyzed *in situ* DRIFTS data. R.C. and M.H.-G. carried out and analyzed all computational work. D.B., T.J.H., M.B.M., K.E.H., T.G., and S.A.F. collected and analyzed the temperature-programmed desorption data. B.R.B. and M.N.D. collected and analyzed the adsorption kinetics data.

### **Competing interests**

The authors have no competing interests to declare.